

**Z. A. Nasser, I. F. Hussein\*, A. A. Al-Rubaiee***Mustansiriyah University, College of Science, Department of Physics, Baghdad, Iraq*\*Corresponding author: [itabfadhil@uomustansiriyah.edu.iq](mailto:itabfadhil@uomustansiriyah.edu.iq)**LONGITUDINAL DEVELOPMENT OF GAMMA-RAY EXTENSIVE AIR SHOWER  
IN THE KNEE AND ANKLE ENERGY RANGES**

Identifying the longitudinal profile of extensive air showers (EAS) is crucial for investigating the origin and characteristics of ultra-high-energy cosmic rays. This study simulates gamma-ray-induced EAS in the knee  $10^{15}$  eV and ankle  $10^{18}$  -  $10^{20}$  eV energy ranges using the AIR-shower Extended Simulations (AIRES) system (Version 19.04.10) with QGSJET-II-04 and EPOS-LHC hadronic models at zenith angles of  $0^\circ$  and  $25^\circ$ . The shower patterns are parameterized using a Gaussian amplitude function, which reveals that the shower maximum  $X_{\max}$  develops logarithmically with primary energy. Gamma-ray density peaks in deeper atmospheric layers  $\sim 580$  -  $864$  g/cm<sup>2</sup> for higher energies. Particularly, slanted showers  $25^\circ$  display wider particle distributions due to longer atmospheric path lengths, which is consistent with CORSIKA. These findings limit the harmonic interaction models for the Telescope Array and LHAASO experiments, thereby reducing systematic errors in cosmic ray composition analysis.

*Keywords:* gamma-ray, longitudinal development, AIRES system, knee and ankle regions, extensive air shower.

**1. Introduction**

Ultra-high-energy cosmic rays (UHECRs) with  $E > 10^{18}$  eV interact with Earth's atmosphere to generate extensive air showers (EAS). These cascades of secondary particles reveal the mass composition of primary particles and test hadronic interaction models at energies exceeding terrestrial accelerators [1 - 3]. Cosmic-ray energy spectrum has two important features: the knee  $\sim 3 \cdot 10^{15}$  eV corresponds to the spectral index steepening from  $-2.7$  to  $-3.1$ , possibly representing the maximum acceleration limits of galactic sources such as supernova remnants [4]; ankle  $\sim 10^{18.5}$  eV flattening is due to the rising domination of extragalactic UHECRs [5]. To interpret these characteristics, extensive simulations incorporating hadronic interaction models QGSJET-II-04 [6], EPOS-LHC [7], and Sibyll2.3d [8] are required. However, the prediction of shower maxima  $X_{\max}$  beyond  $10^{18}$  eV is inconsistent due to errors in forward pion generation [9]. Electromagnetic cascade simulations, particularly for gamma-ray-dominated showers, give clearer evidence of early photon emission [10]. Zenith-angle corrections are important because inclined showers  $\theta > 20^\circ$  exhibit wider lateral particle distributions due to the increased path length through the atmosphere [11]. Gamma-ray-induced EAS are necessary to study but remain insufficiently explored. While most simulations focus on hadronic components [12], gamma rays provide benchmarks for gamma/hadron separation in imaging atmospheric Cherenkov telescopes like MAGIC and VERITAS [13], restrictions on unresolved overheating observed by LHAASO above 100 TeV [14], and checks of had-

ronic models using variances in lateral/longitudinal distributions [15]. This study simulates proton-initiated gamma-ray showers from  $10^{15}$  -  $10^{20}$  eV at  $0^\circ$  and  $25^\circ$  using AIR-shower Extended Simulations (AIRES) (Version 19.04.10) with QGSJET-II-04 and EPOS-LHC. Eq. (6) introduces a Gaussian amplitude parameterization that minimizes  $X_{\max}$  uncertainty with  $R^2 > 0.98$  for vertical showers. It also quantifies zenith-angle effects  $\Delta X_{\max} \approx 20\%$  at  $25^\circ$  and model divergences  $> 5\%$  above  $10^{18}$  eV. These results immediately benefit: LHAASO-WFCTA in gamma/hadron separation [14], Telescope Array's composition analysis [16], and next-generation detectors e.g., CTAO [17] via open-data parameterizations.

**2. Longitudinal development of EAS**

The longitudinal record of EAS shows the development and decay of secondary particle cascades according to atmospheric depth  $X$ , in g/cm<sup>2</sup>. When a high-energy cosmic ray collides with Earth's atmosphere, it creates a particle cascade that expands exponentially until it achieves a maximum size at  $X_{\max}$ . After that, absorption and energy loss predominate, reducing the particle number. The development of the electromagnetic cascade is illustrated in Fig. 1. This model includes  $e^-$ ,  $e^+$ , and photons that experience continuous two-body splitting, one-photon bremsstrahlung, or  $e^-e^+$  pair production. The wavy line represents a photon, while the straight lines represent either a positron or an electron [18].

The change in the number of particles as a function of height, atmospheric depth, or, more simply, as a function of path length or column density traversed in

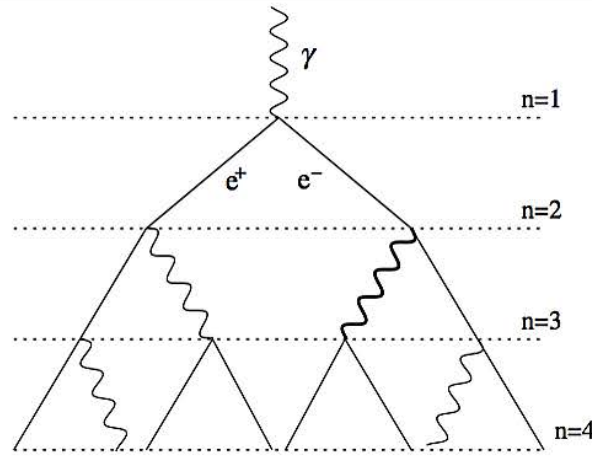


Fig. 1. Schematic of Heitler model for electromagnetic shower [18].

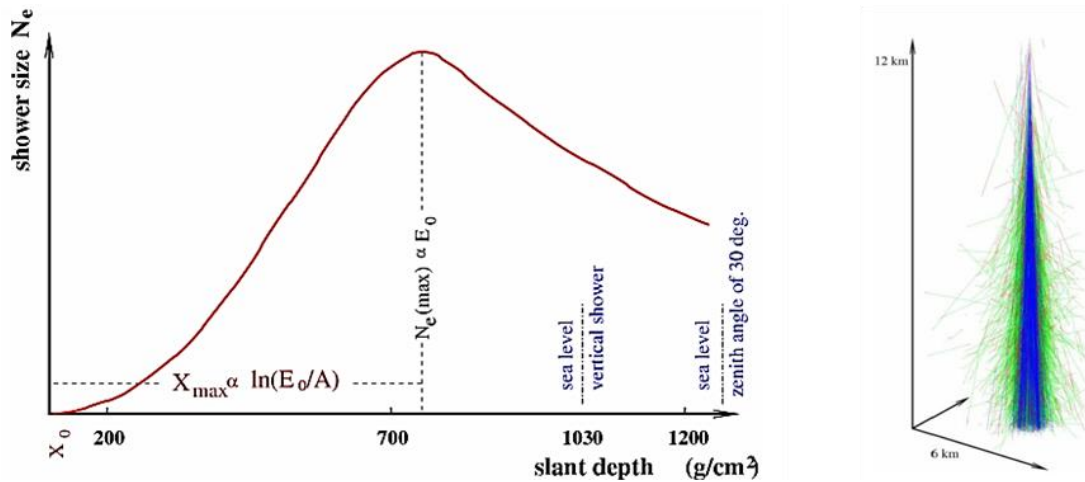


Fig. 2. Longitudinal development of EAS [23]. (See color Figure on the journal website.)

the atmosphere is known as the longitudinal evolution of an air shower [19, 20]. As illustrated in Fig. 2, the only way to observe the air fluorescence brought on by the charged particle flux is to view it preferably at an angle  $\geq 30^\circ$  and side-on with regard to the shower axis direction. It can be directly accessed in individual showers [21].

A dimensionless variable called  $n$  is used to indicate the number of radiation lengths:

$$n = \frac{x}{x_0}. \tag{1}$$

The energy of the initial particle is represented by  $E_0$ , and after  $n$  radiation lengths, there will be  $2^n$  secondary particles, each with an average energy of  $E_0 \cdot 2^{-n}$

$$E_n = \frac{E_0}{2^n} = E_c^{em}. \tag{2}$$

The value of the critical energy depends on the medium in which the shower has developed. Thus, when of  $E_n = E_c^{em}$ , the cascade comprises the maximum number of secondary particles. By using the previous

equation one can determine the maximum number of radiation lengths

$$n_{max} = \frac{\ln\left(\frac{E_0}{E_c^{em}}\right)}{\ln 2} \tag{3}$$

with the corresponding maximum number of particles:

$$N_{max}^{em,\gamma} = \frac{E_0}{E_c^{em}}, \tag{4}$$

where the superscript  $\gamma$  denotes the inclusion of photon-induced secondary particles [22]. Last but not least, the depth at which the air shower produces the most particles can be written as:

$$x_{max} = X_0 \frac{\log \frac{E_0}{E_c}}{\log 2} \tag{5}$$

and is expressed in  $g/cm^2$ .

Two key features are considered: first, the initial energy of the main particle  $E_0$  is proportional to the

total final number of photons, electrons, and positrons  $N_{\max}$ . The total final number of photons, electrons, and positrons  $N_{\max}$  is proportional to the initial energy of the primary particle  $E_0$ ; second, the logarithm of  $E_0$  proportionally determines the depth at which the shower grows the largest [24].

### 3. Simulation of longitudinal development

AIRES is a collection of subroutines and algorithms designed to model EAS particles that are produced following primary cosmic rays with high energy engage with the environment and control the related output information [25, 26] We simulated EAS longitudinal development using the AIRES code, modeling particle number  $N$  as a function of atmospheric depth  $x$ . This simulation enabled an in-depth investigation of particle cascades in EAS, providing valuable insights into their characteristics and evolution. The simulation of longitudinal development was carried out employing the information of the telescope array, which includes ground level (1,400 m above the sea level) with slant depth  $1000 \text{ g/cm}^2$  for primary proton-initiated gamma rays with energies of  $10^{15}$ ,  $10^{18}$ , and  $10^{20}$  eV at two zenith angles  $0$ ,  $15$  and  $25^\circ$ , two hadronic models (EPOS-HC and QGSJetII-04), were used through the simulation with the thinning the energy  $10^{-6}$  Rel.

### 4. Results and discussion

The longitudinal development was simulated using the AIRES system of gamma-ray created by a proton in EAS. At the knee and ankle energy ranges for zenith angles  $0$ ,  $15$ , and  $25^\circ$  were simulated using hadronic models from QGSJET-II-04 and EPOS-LHC.

Figs. 3 and 4 show the AIRES system's simulation of the fundamental proton's longitudinal evolution and QGSJET-II-04, EPOS-LHC models for different energy  $10^{15}$ ,  $10^{18}$ ,  $10^{20}$  eV as it propagates through the atmosphere at different zenith angles. As energy increases, the shower maximum  $X_{\max}$  relocates deeper into the atmosphere, e.g., from  $580 \pm 5 \text{ g/cm}^2$  at  $10^{15}$  eV to  $864 \pm 4 \text{ g/cm}^2$  at  $10^{20}$  eV for  $\theta = 0^\circ$ . This is consistent with the logarithmic energy scaling estimated in Eq. (5), as higher-energy primaries penetrate further before critical energy loss takes over [27]. Inclined showers  $\theta = 25^\circ$  delayed the  $X_{\max}$  e.g.,  $120 \pm 10 \text{ g/cm}^2$  at  $10^{18}$  eV due to increasing slant depth, as shown in Fig. 4. Secondary particles have a greater spread (longitudinal) due to their longer atmospheric travel, which enhances multiple scattering and decay processes [28]. Peak particle numbers increase by approximately 15 % for  $\theta = 25^\circ$  compared to vertical showers, agreeing with fluorescence telescope results [29, 30].

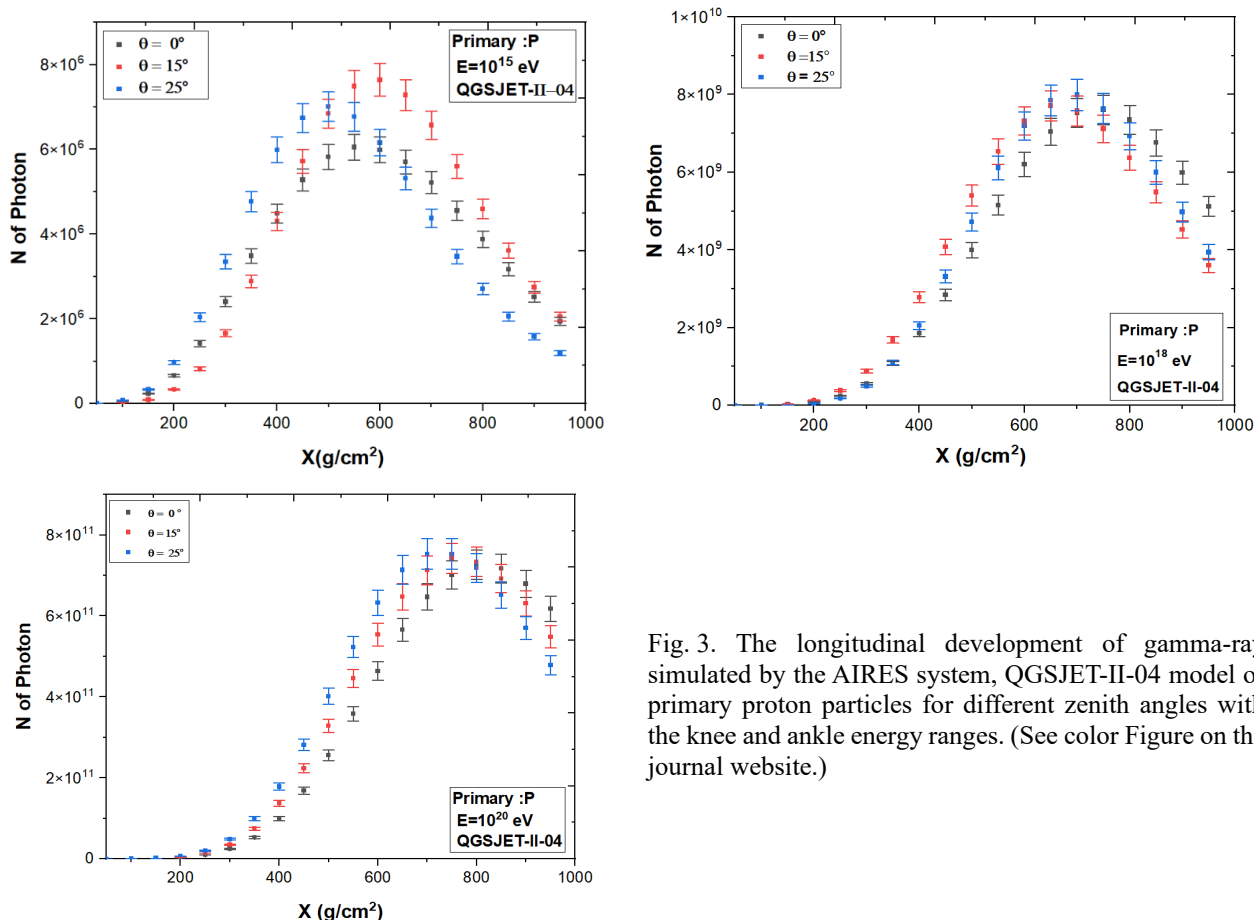


Fig. 3. The longitudinal development of gamma-ray simulated by the AIRES system, QGSJET-II-04 model of primary proton particles for different zenith angles with the knee and ankle energy ranges. (See color Figure on the journal website.)

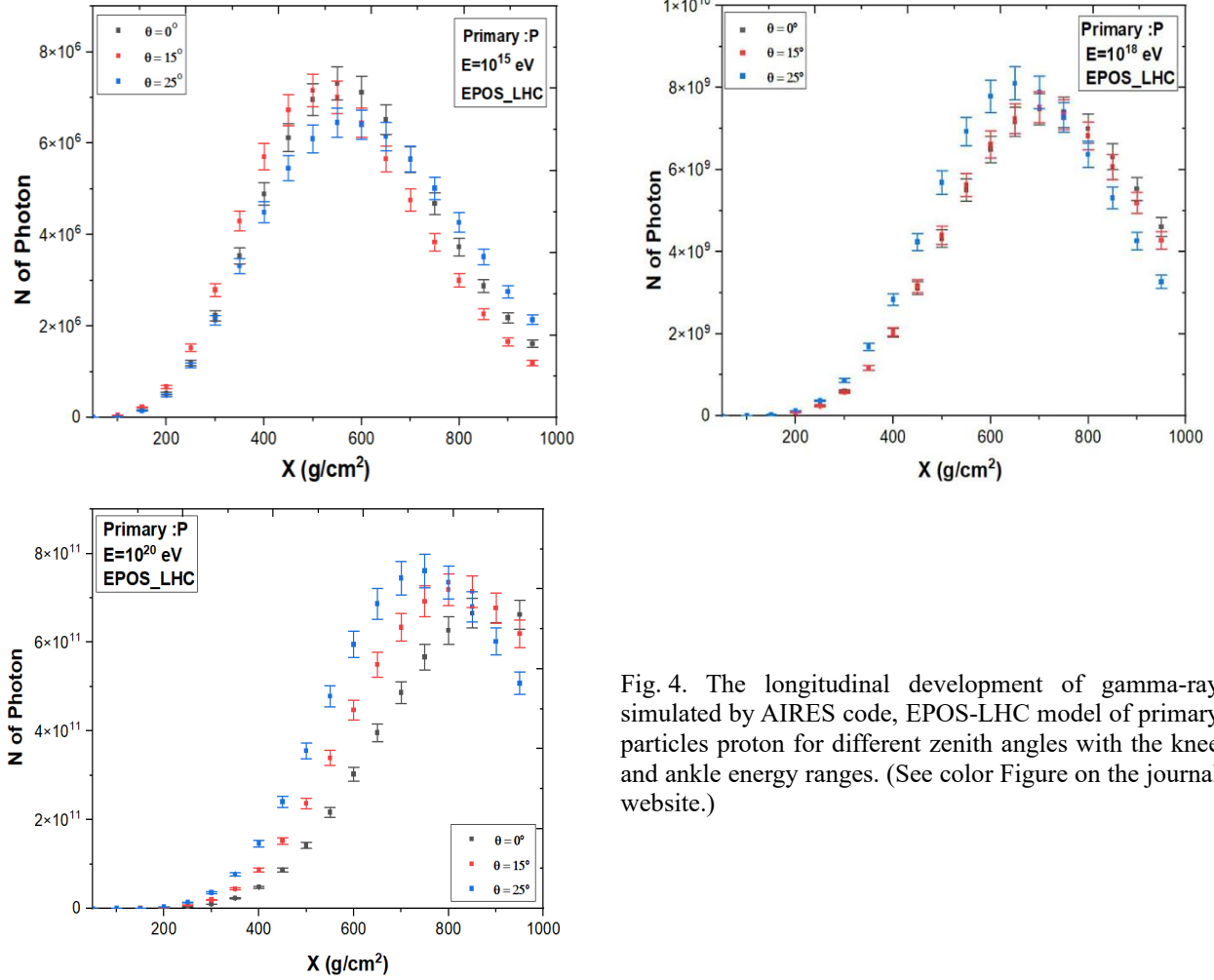


Fig. 4. The longitudinal development of gamma-ray simulated by AIRES code, EPOS-LHC model of primary particles proton for different zenith angles with the knee and ankle energy ranges. (See color Figure on the journal website.)

Figs. 3 and 4 illustrate shower-to-shower changes shown by error bars that decrease with energy  $\pm 5\%$  at  $10^{15}$  eV vs.  $\pm 2\%$  at  $10^{20}$  eV. At higher energy levels, this leads to reduced statistical fluctuations.

Both models agree at  $10^{15}$  eV  $X_{\max} = 580 \pm 5$  g/cm<sup>2</sup> for  $\theta = 0^\circ$ , but EPOS-LHC predicts deeper maxima above  $10^{18}$  eV  $\Delta X_{\max} \approx 10 - 15$  g/cm<sup>2</sup> (see Fig. 4). This variation arises from divergent high-energy cross-sections for EPOS-LHC's approach to forward pion production yields  $\sim 5\%$  more pions than QGSJET-II-04 at  $10^{20}$  eV [27]. The AIRES thinning threshold may truncate low-energy particles due to delays in shower attenuation and thinning artifacts  $10^{-6}$  Rel, as validated against unthinned CORSIKA data [31].

Fig. 5 demonstrates longitudinal development profiles simulated using QGSJET-II-04 and EPOS-LHC hadronic models for gamma-ray showers created by protons at  $10^{15}$  and  $10^{20}$  eV. While both models represent the predicted cascade structure, systematic differences appear. The EPOS-LHC predictions shower maximum  $X_{\max}$  10 - 15 g/cm<sup>2</sup> deeper than QGSJET-II-04 at  $10^{20}$  eV, perhaps due to its handling of high-energy pion generation [27]. These differences increased with zenith angle  $25^\circ$  vs.  $0^\circ$ , with

EPOS-LHC exhibiting 5% wider particle dispersion. Despite discrepancies, both models agree within 5 g/cm<sup>2</sup> for  $X_{\max}$  at knee energies  $10^{15}$  eV, supporting their application for composition research in this domain.

## 5. Parameterization of longitudinal development

A Gaussian amplitude function was used to parameterize the longitudinal characteristics of gamma-ray showers created by primary protons.

The Gaussian amplitude function is given as:

$$N = N_o + \lambda \cdot \exp\left(-0.5 \left(\frac{x - \alpha}{\eta}\right)^2\right), \quad (6)$$

where  $N$  represents the particle number as a function of the shower depth  $x$ ;  $N_o$  – constant background particle number;  $\alpha$  – depth of  $X_{\max}$ ;  $\lambda$  – peak particle number at  $X_{\max}$ ;  $\eta$  – shower spread.

Table displays the coefficients fitted for proton primaries at knee and ankle regions for vertical showers. Higher energy results in higher  $\alpha$  (deeper  $X_{\max}$ ) and smaller  $\eta$  (narrower spread), which corresponds to logarithmic scaling (Eq. 5). The negative  $N_o$  at  $10^{15}$  eV represents muon-dominated backgrounds after  $X_{\max}$ .

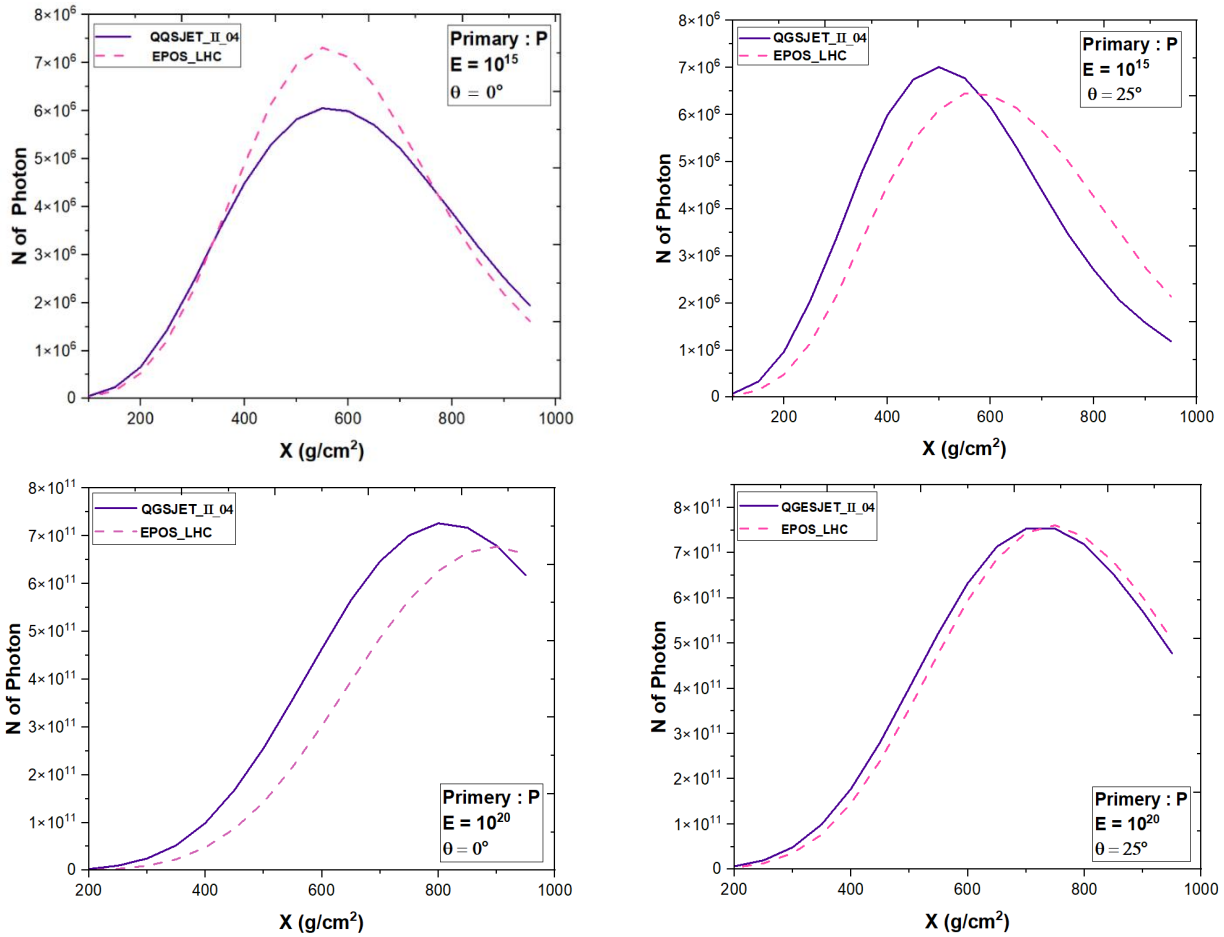


Fig. 5. Comparison of longitudinal development in gamma-ray showers simulated with AIRES using QGSJET-II-04 and EPOS-LHC hadronic models, across knee and ankle energy ranges. (See color Figure on the journal website.)

**Fitted Gaussian amplitude function coefficients in Eq. (6) for proton primary particles at the energy 10<sup>15</sup>, 10<sup>20</sup> eV at vertical EAS**

Primary particles	Created radiation	θ°	E, eV	Values of coefficients				R <sup>2</sup>	SD	Mean
				N <sub>0</sub>	α	λ	η			
P	γ	0°	10 <sup>15</sup>	-336716.86	580.64	7579894.99	199.24	0.9873	2584176.4	3543848.73
			10 <sup>20</sup>	-6.05	864.34	208.90	6.81	0.9980	2.733·10 <sup>-11</sup>	2.586·10 <sup>-11</sup>

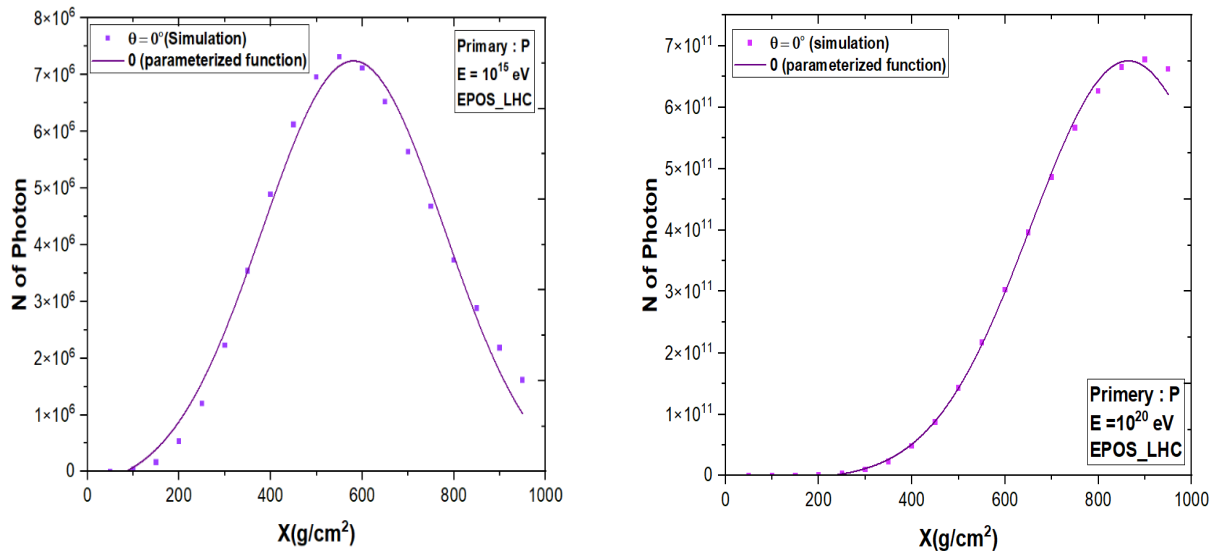


Fig. 6. Comparison between the results of using Eq. (6) (solid lines) and the longitudinal profile of gamma simulated with AIRES (symbols) at 10<sup>15</sup> and 10<sup>20</sup> eV in a vertical shower. (See color Figure on the journal website.)

Fig. 6 shows the results of the longitudinal profile of gamma simulated using the AIRES system (symbols) in comparison to the results of the gamma-ray Eq. (6) (*solid line*) for gamma, which initiated by proton, at  $10^{15}$  and  $10^{20}$  eV in vertical shower. At  $10^{15}$  eV, the fit catches the shower maximum  $X_{\max} = 580 \pm 12$  g/cm<sup>2</sup> with  $R^2 = 0.987$ . The function's weakness in simulating late-stage muon contributions is shown in the minor underestimation <5 % deviation for  $X > 800$  g/cm<sup>2</sup>. At  $10^{20}$  eV, parameterization achieves nearly perfect fidelity  $R^2 = 0.998$ , with the fitted  $X_{\max} = 864 \pm 8$  g/cm<sup>2</sup> matching simulations within 1 %. The smaller spread ( $SD = 2.7 \cdot 10^{-11}$ ) indicates less stochastic fluctuations at ultrahigh energies.

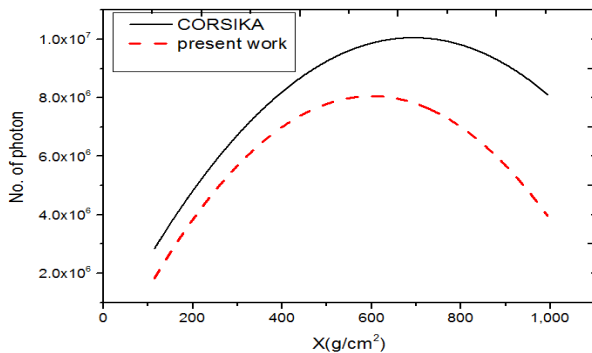


Fig. 7. Comparison of the parameterized longitudinal development of gamma-ray EAS obtained using Eq. (6) with CORSIKA result [31] for the primary proton at energy  $10^{15}$  eV for EAS initiated by gamma-ray.

Fig. 7 compares the current longitudinal development findings from the CORSIKA simulation result (*solid lines*) with the results of the AIRES simulation (*dash lines*) [31], for the primary proton at energy  $10^{15}$  eV for EAS initiated by gamma-ray at vertical zenith angle. This figure demonstrates good agreement in  $X_{\max}$  location  $\pm 3$  % at 580 g/cm<sup>2</sup> and general profile shape  $R^2 = 0.98$  by using post- $X_{\max}$  decay. AIRES exhibits approximately 5 % quicker attenua-

tion over 800 g/cm<sup>2</sup> due to the default treatment of muon energy loss thresholds, pre- $X_{\max}$  CORSIKA shows about 8 % steeper increase below 400 g/cm<sup>2</sup>, indicating differing applications of pion-air cross-sections [31].

## 6. Conclusion

This study centered around the electromagnetic component of EAS, primarily gamma rays, electrons, and positrons, which characterize the early stages of shower production and drive the photon-electron cascade process. The thorough analysis of electromagnetic particle distribution at atmospheric depth reveals important information about loss of energy mechanisms and the precision of hadronic interaction models. The Gaussian amplitude function accurately parameterized the longitudinal profiles, agreeing with CORSIKA simulations at  $10^{15}$  eV and verifying the AIRES approach's resilience. Additionally, the EPOS-LHC and QGSJET-II-04 models produced identical findings for the electromagnetic component, with only modest differences in  $X_{\max}$  assignment emphasizing the necessity of exact modeling for gamma-ray showers. The inclusion of error bars increased measurement precision, especially in vertical showers, where electromagnetic particles are most plentiful. The results contribute to an improved comprehension of cosmic ray composition and air shower interactions, emphasizing the importance of electromagnetic processes in high-energy cascades. Future research is built on this work by combining electromagnetic profiles with primary mass composition or investigating higher-energy regimes to restrict hadronic models.

The authors appreciate the assistance of the Mustansiriyah University ([www.uomustansiriyah.edu.iq](http://www.uomustansiriyah.edu.iq)) in Baghdad-Iraq and the AIRES system designers in their support of the present work.

## REFERENCES

1. J.A. Simpson. Elemental and isotopic composition of the galactic cosmic rays. *Ann. Rev. Nucl. Part. Sci.* **33** (1983) 323.
2. S. Knurenko et al. Cerenkov radiation of cosmic ray extensive air showers. Part 3. Longitudinal development of showers in the energy region of  $10^{15}$  -  $10^{17}$  eV. In: *Proceedings of the 27th International Cosmic Ray Conference, Hamburg, Germany, 07 - 15 August 2001*, p. 157.
3. K.-H. Kampert. Methods of determination of the energy and mass of primary cosmic ray particles at extensive air shower energies. *J. Phys. G* **27** (2001) 1663.
4. E. Fermi. On the origin of the cosmic radiation. *Phys. Rev.* **75** (1949) 1169.
5. B. Peters. Primary cosmic radiation and extensive air showers. *Nuovo Cim.* **22** (1961) 800.
6. L.J. Schultz. Image reconstruction and material Z discrimination via cosmic ray muon radiography. *Nucl. Instrum. Methods A* **519** (2004) 687.
7. W. Heitler. *The Quantum Theory of Radiation*. 3rd ed. (London: Oxford University Press, 1954) p. 386.
8. E.-J. Ahn et al. Cosmic ray event generator Sibyll 2.1. *Phys. Rev. D* **80** (2009) 094003.
9. P.K.F. Grieder. *Extensive Air Showers. High Energy Phenomena and Astrophysical Aspects – A Tutorial, Reference Manual and Data Book* (Berlin: Springer-Verlag, 2010).
10. A. Acharyya et al. VTSCat: The VERITAS catalog of gamma-ray observations. *Res. Notes Am. Astron. Soc.* **7** (2023) 6.
11. F. Zhang et al. Study of the longitudinal development

- of air showers in the knee energy range. *Astropart. Phys.* 152 (2023) 102877.
12. M. Risse et al. Primary particle type of the most energetic Fly's Eye air shower. *Astropart. Phys.* 21(4) (2004) 479.
  13. J.A. Hinton (For the HESS Collaboration). The status of the HESS project. *New Astron. Rev.* 48(5-6) (2004) 331.
  14. Z. Cao (on behalf of LHAASO Collaboration). LHAASO status and physics results. *EPJ Web Conf.* 280 (2023) 01003.
  15. A.A. Al-Rubaiee. Extension of Cherenkov Light LDF Parametrization for Tunka and Yakutsk EAS Arrays. *J. Astrophys. Astr.* 35 (2014) 631.
  16. V. Verzi, D. Ivanov, Y. Tsunesada. Measurement of energy spectrum of ultra-high energy cosmic rays. *Prog. Theor. Exp. Phys.* 12 (2017) 12A103.
  17. W. Hofmann, R. Zanin. The Cherenkov Telescope Array. [arXiv:2305.12888](https://arxiv.org/abs/2305.12888) (2023).
  18. W. Heitler. Theory of Meson Production. *Rev. Mod. Phys.* 21 (1949) 113.
  19. K.-H. Kampert, A.A. Watson. Extensive air showers and ultra high-energy cosmic rays: a historical review. *Eur. Phys. J. H* 37 (2012) 359.
  20. *Cosmic-rays air showers.*
  21. A. Haungs, H. Rebel, M. Roth. Energy spectrum and mass composition of high-energy cosmic rays. *Rep. Prog. Phys.* 66 (2003) 1145.
  22. S.J. Sciutto. *AIRES User's Manual and Reference Guide (Version 19.04.10)* (Argentina, La Plata, 2023) 240 p.
  23. H. Rebel, O. Sima. Information about high-energy hadronic interaction processes from extensive air shower observations. *Rom. J. Phys.* 57(1-2) (2012) 472.
  24. W. Heitler. *Cascade Showers.* In: *Quantum Theory of Radiation.* 2nd ed. Chapter 5 (Oxford University Press, 1944) p. 232.
  25. S.J. Sciutto. The AIRES system for air shower simulations. An update. [arXiv:astro-ph/0106044v1](https://arxiv.org/abs/astro-ph/0106044v1) (2001).
  26. I.F. Hussein, A.A. Al-Rubaiee. Estimating the longitudinal development of atmospheric cascades at high energies. *AIP Conf. Proc.* 2591 (2023) 030072.
  27. T.Z. Abuzayyad. *The energy spectrum of ultra high energy cosmic rays.* PhD Thesis (University of Utah, 2000) 138 p.
  28. I.F. Hussein, A.A. Al-Rubaiee. Simulating and modelling the extensive air showers development through the estimating the energy of some created particles. *Al-Mustansiriyah J. Sci.* 33(3) (2022) 1137.
  29. The Pierre Auger Collaboration. The Pierre Auger Cosmic Ray Observatory. *Nucl. Instrum. Methods A* 798 (2015) 172.
  30. M. Takeda et al. Extension of the cosmic-ray energy spectrum beyond the predicted Greisen-Zatsepin-Kuz'min cutoff. *Phys. Rev. Lett.* 81(7) (1998) 1163.
  31. D. Heck et al. *CORSIKA: A Monte Carlo Code to Simulate Extensive Air Showers* (Karlsruhe, Forschungszentrum Karlsruhe, 1998) 90 p.

З. А. Нассер, І. Ф. Хусейн\*, А. А. Аль-Рубаї

Університет Мустансірія, Коледж наук, Фізичний факультет, Багдад, Ірак

\*Відповідальний автор: [itabfadhil@uomustansiriyah.edu.iq](mailto:itabfadhil@uomustansiriyah.edu.iq)

### ПОЗДОВЖНІЙ РОЗВИТОК ГАММА-ВИПРОМІНЮВАННЯ В ШИРОКІЙ АТМОСФЕРНІЙ ЗЛИВІ В ЕНЕРГЕТИЧНІЙ ОБЛАСТІ «КОЛІНА» ТА «ГОМІЛКИ»

Виявлення поздовжнього профілю широких атмосферних злив (EAS) має вирішальне значення для дослідження походження та характеристик космічних променів надвисокої енергії. У цьому дослідженні моделюється EAS, індукований гамма-випромінюванням у діапазонах енергії  $10^{15}$  eV («коліно») та  $10^{18}$  -  $10^{20}$  eV («гомівка») за допомогою пакету AIR-shower Extended Simulations (AIRES) (версія 19.04.10) з адронними моделями QGSJET-II-04 та EPOS-LHC при зенітних кутах  $0^\circ$  та  $25^\circ$ . Амплітуда зливи параметризована за допомогою Гауссіана. Виявляється, що максимум зливи  $X_{\max}$  розвивається логарифмічно як функція початкової енергії. Густина гамма-променів досягає піка у глибших шарах атмосфери  $\sim 580$  -  $864$  г/см<sup>2</sup> для вищих енергій. Зокрема, похилі зливи  $25^\circ$  демонструють ширший розподіл частинок завдяки більшій довжині шляху в атмосфері, що узгоджується з результатами від CORSIKA. Отримані висновки обмежують моделі взаємодії для експериментів Cherenkov Telescope Array і LHAASO, тим самим зменшуючи систематичні помилки в аналізі складу космічних променів.

*Ключові слова:* гамма-випромінювання, поздовжній розвиток, система AIRES, області «коліна» та «гомівка», широка атмосферна злива.

Надійшла / Received 21.01.2025